Template effects on the pressure-dependent behavior of chabazite-type fluoroaluminophosphates: A computational approach

Michael Fischer[a,b]

a) University of Bremen, Crystallography Group, Department of Geosciences,

Klagenfurter Straße 2-4, 28359 Bremen, Germany.

b) University of Bremen, MAPEX Center for Materials and Processes,

28359 Bremen, Germany

E-mail: michael.fischer@uni-bremen.de

Phone: 0049-421-28165163

ORCID: 0000-0001-5133-1537

Abstract

Experimental in-situ studies have shown that the compressional behavior of zeolite frameworks depends not only on the framework topology, but also on the extra-framework content, i.e. the species residing in the pores (cations, water molecules, templates). However, systematic experimental studies of isotypic frameworks with different extra-framework content often face several challenges, such as limited quality of the diffraction data and non-ideal behavior of the pressure-transmitting medium. In order to provide an alternative computational perspective, the compressional behavior of four fluoroaluminophosphate zeolite analogues with a chabazite (CHA) topology was investigated using electronic structure calculations in the framework of dispersion-corrected density functional theory (DFT). The AlPO-CHA systems differ in the nature of the organic template molecule occupying the chabazite cage, with the template species being morpholinium (morph), pyridinium (pyr), dimethylimidazolium (DMI), and trimethylimidazolium (TMI), respectively. For the case of AlPO-CHA_morph, the evolution of the lattice parameters with pressure as obtained from the computations was found to be in agreement with experimental data from an earlier in-situ diffraction investigation. In particular, the occurrence of a structural transition at pressures above 3 GPa could be reproduced. An analysis of the DFT-optimized structures showed that a pronounced elongation of the chabazite cage occurs upon the transition, which is associated with a rearrangement of the morpholinium molecules residing in the cage. Moreover, the double six-ring building units are strongly deformed during the transition. Analogous computations for the other three AlPO-CHA systems showed no indications for the occurrence of a *P*-induced transition, with only minor discontinuities in the evolution of the structural parameters with pressure. The compressibility in the low-pressure range varied widely depending on the template, with bulk moduli ranging from 19 GPa for AlPO-CHA_pyr to 51 GPA for AlPO-CHA_TMI. Despite the identical composition of the framework, different deformations of the double six-ring units with pressure were observed. The present study highlights the important

influence of the template on the compressional behavior of porous framework compounds. Firstly, the molecular volume of the template and the nature of the framework-template interactions impact upon the compressibility in the low-pressure regime. Secondly, the ability of the template to accommodate pressure through continuous rotation and shortening of template-template and framework-template distances determines whether a discontinuous structural transition occurs or not.

Keywords

zeolites, high-pressure studies, density functional theory, host-guest interactions

Introduction

The response of inorganic tetrahedral framework materials to pressure has been widely studied in the last ~20 years (Gatta and Lee 2014; Gatta et al. 2018). By virtue of their intrinsic porosity and the possibility to adsorb (and desorb) guest molecules, zeolites are a particularly important group of tetrahedral frameworks in a materials science context, where they find technological applications in ion exchange, adsorption, and catalysis, among other fields (Masters and Maschmeyer 2011). Moreover, several zeolites occur as natural minerals as a product of hydrothermal, diagenetic or low-grade metamorphic processes, rendering their response to pressure interesting in a geoscientific context (Passaglia and Sheppard 2001). In a recent review of high-pressure studies of zeolites, Gatta et al. distinguished four key areas of study of their *P*-dependent behavior (Gatta et al. 2018): (1) Compressional behavior and *P*-induced deformation mechanisms, (2) *P*-induced intrusion of guest molecules, (3) *P*-dependent variations of the ionic conductivity, and (4) *P*-induced amorphization. With regard to the compressional behavior, different zeolites span a rather large range of bulk moduli, from ~15 to 70 GPa (Gatta and Lee 2014). On the one hand, the compressibility is related to the framework type, as different frameworks have different abilities to respond to pressure, with the dominant rearrangements in the *P* range up to ~5 GPa being related to a tilting of TO_4 tetrahedra with respect to each other (this typically corresponds to a decrease of T-O-T angles with increasing pressure). Deformations of TO_4 tetrahedra and contraction of T-O bonds normally become significant only at higher pressures. On the other hand, even isotypic frameworks may exhibit very different compressibilities, depending on the presence and nature of extra-framework species residing in the cavities (charge-balancing cations, water molecules, organic templates). If the pressure-transmitting medium used in the in-situ experiments is able to enter the zeolite pores (i.e. it is a "penetrating" fluid), the interaction between framework and pressure-transmitting fluid will also affect the *P*-dependent behavior observed experimentally (Gatta et al. 2018). Zeolite structures for which the *P*-dependent behavior has been studied using in-situ diffraction techniques range from

structurally fairly simple systems like Li-ABW, which has a unit cell volume of ~400 $Å^3$ and eight atoms in the asymmetric unit (Fois et al. 2008), to very complex zeolites like the natural mineral paulingite, which has a cubic unit cell with an edge length of ~35 Å (volume >40,000 $Å^3$) and more than 40 atoms in the asymmetric unit (Gatta et al. 2015).

Zeolites with a chabazite framework (framework type code CHA) occur as natural minerals, but they are also accessible synthetically for a variety of chemical compositions: In the domain of aluminosilicates (where T = Si, Al), compositions ranging from low Si/Al ratios to pure-SiO_2 can be synthesized. Moreover, it is also possible to synthesize CHA-type systems as aluminophosphates (AlPOs – T = Al, P) and as heteroatom-substituted AlPO derivatives (e.g. silicoaluminophosphates – SAPOs). The CHA framework can be described as an AABBCC stacking of six-membered rings, i.e. rings consisting of six T atoms. The two composite building units are barrel-shaped double six-ring units (*d6r* units in the nomenclature of the International Zeolite Association (Baerlocher et al. 2007)) and chabazite (*cha*) cages. The elliptical *cha* cages, which have dimensions of roughly 7 × 10 Å, are connected by eight-ring windows with a diameter of ~3.8 Å. The pressure response of CHA-type systems has been investigated in a series of in-situ diffraction studies by Leardini et al. (Leardini et al. 2010; Leardini et al. 2012; Leardini et al. 2013). The first paper of this series reported results on a natural chabazite sample, where the cages are occupied by cations (mainly potassium and calcium) and water molecules, and on SAPO-34, a silicoaluminophosphate containing morpholinium cations and water (Leardini et al. 2010). Lattice parameters were refined up to 7.6 GPa for the natural sample, and up to 4.5 GPa for SAPO-34, delivering a much lower compressibility for the former system, with bulk moduli of 61 GPa and 29 GPa, respectively. Moreover, the observed evolution of the lattice parameters was also different: In natural chabazite, the compression along the hexagonal *a*-xis is more pronounced than along *c*. In SAPO-34, *c* decreases more markedly than *a* up to 2 GPa, and increases slightly above this pressure. The authors attributed this change in slope to the effect of the bulky morpholinium cations, which prevent a

further compression of the *cha* cage along this axis. The lower compressibility of the natural chabazite was explained with a more complete filling of the cage by extra-framework species. A subsequent study of triclinic AlPO-34, which also contains morpholinium cations, revealed a marked discontinuity in the evolution of the lattice parameters between 3.1 and 3.9 GPa, where the length of the pseudo-hexagonal *c*-axis increases by ~4%, whereas the *a*-axes shrink (Leardini et al. 2012). Despite the absence of water molecules in the cages, the compressibility of AlPO-34 is lower than that of the water-containing SAPO-34, with a bulk modulus of 54 GPa in the pressure range from 0.4 to 3.1 GPa (above this pressure, the unit cell volume shows a non-linear evolution, and no bulk modulus was calculated). In the last paper from that series, another natural chabazite sample was studied (Leardini et al. 2013). Between pressures of 2.1 and 2.5 GPa, a rhombohedral-to-triclinic phase transition occurs, which is associated with a drop in unit cell volume by about ~4%. The compressibility of the rhombohedral phase is comparable to that of the natural chabazite mentioned above, with a bulk modulus of 54 GPa, but the triclinic high-pressure phase is significantly stiffer (bulk modulus of 91 GPa). Unlike in the previous study, the data quality permitted a refinement of the structures for pressures up to 1.1 GPa. On that basis, Leardini et al. were able to analyze the structural deformation mechanisms: In particular, the marked decrease of the *c*-axis upon compression was found to be associated with a) a flattening of the *d6r* building units and b) an increasing circularity of the eight-ring windows.

While experimental studies using in-situ diffraction at elevated pressures have delivered various important insights into the *P*-dependent behavior of zeolite frameworks, the information obtained from such studies does not always allow for a complete microscopic understanding. As mentioned above, limited quality of the diffraction data may prevent a refinement of the atomic coordinates. Moreover, the intrusion of guest molecules and the non-hydrostatic behavior of the *P*-transmitting media above a certain pressure put limitations on the pressure range that is accessible experimentally under essentially “ideal” conditions. To this end, computational modelling methods,

which are able to study ideal model systems, can provide additional insights that may be difficult or impossible to obtain via an experimental route. Besides geometric methods, which employ a simplified representation of the structure (Wells and Sartbaeva 2015), atomistic modelling techniques can be used. These include force-field based methods, which use empirical parameters to describe interatomic interactions (Combariza et al. 2013), and "first-principles" electronic structure methods like density functional theory (DFT).

As a recent comprehensive review covering both experimental and theoretical works is available (Gatta et al. 2018), we mention only a few example applications of DFT to the study of elastic properties of zeolites: DFT-based ab-initio Molecular Dynamics (AIMD) calculations in conjunction with synchrotron powder diffraction experiments were employed to study the pressure dependent behavior of hydrated Li-ABW (Fois et al. 2008). As only the unit cell parameters could be refined from the experimental data, the calculations were pivotal to develop a microscopic understanding of the deformation mechanism. In addition to an increasing elliptical deformation of the one-dimensional channels, the hydrogen bonding pattern of the water molecules changes with pressure. On the other hand, the coordination of the Li cations remains essentially unaffected. The same groups used an analogous approach to study the zeolite mineral gismondine (Betti et al. 2007). For this system, an increase of the average coordination number of the calcium cations upon increasing pressure was observed, and changes in the coordination environment of the cations between pressures of 2 and 3 GPa correlate with a discontinuity in the evolution of some of the lattice parameters. AIMD calculations also revealed a fundamental impact of the extra-framework content on the compressional behavior of the Ca-containing zeolite yugawaralite (Fois et al. 2005). In a rather different direction, Coudert performed a DFT-based screening of the elastic properties of more than 100 all-silica zeolites (Coudert 2013). While many frameworks were found to have highly anisotropic elastic properties, those that are synthetically accessible in all-silica form tend to be mechanically fairly stable, and exhibit only modest anisotropy.

In this work, dispersion-corrected DFT calculations are employed to study the *P*-dependent behavior of four CHA-type fluoroaluminophosphates containing different organic templates up to a pressure of 5 GPa. In the following, we describe the model systems and the computational approach. Afterwards, the performance of different "flavours" of DFT in reproducing structural data and, where available, the bulk modulus is assessed. The best-performing approach is then used to study the structural evolution of the morpholinium-containing AlPO-CHA system, for which lattice parameters (but no atomic coordinates) at non-ambient pressures have been refined from experimental data. In order to study the influence of the template species on the compressional behavior, analogous calculations are performed for three other AlPO-CHA materials. The resulting structures are analyzed in detail to obtain a microscopic picture of the structural deformations upon pressure increase.

Model systems and computational methods

Overview of AlPO-CHA systems

Four CHA-type fluoroaluminophosphates were considered in this study, all of which have the unit cell composition $Al_6P_6O_{24}F_2 \cdot 2(templ)$, where *templ* represents the positively charged organic template molecules. A single unit cell contains one *d6r* unit and one *cha* cage, with each cage being occupied by two template molecules. The charge of the templates is balanced by two fluoride anions that are bonded to Al atoms located at opposite vertices of a four-ring connecting two *d6r*

units (Fig. 1). In fluoride-containing all-silica zeolites, fluoride anions are typically found in small cages, e.g. in SiO_2-CHA, where they are located inside the *d6r* units (Villaescusa et al. 2003). In fluoroaluminophosphates, fluoride anions may either occupy small cages, especially double four-ring (*d4r*) units, or form Al-F-Al bridges between Al atoms that are part of the same four-ring (Loiseau and Férey 2007). In the AlPO-CHA systems studied here, this "bridging" arrangement has two fluoride anions in relatively close proximity, with F-F distances in the range of 2.4 Å (Fig. 1 b). While this might incur non-negligible anion-anion repulsion, it also allows for a simultaneous interaction of each fluoride anion with two Al atoms, with both Al-F distances having similar length (~1.9 Å). Because the Al-O bonds have a more ionic character than the P-O bonds, which are dominantly covalent (Corà and Catlow 2001), the aluminum atoms are more susceptible towards an expansion of their coordination number from four to five or – as observed here – six (AlO_4F_2 octahedra).

Due to the presence of fluoride anions and template molecules and the associated distortions, the symmetry of the CHA-type fluoroaluminophosphates is reduced from the rhombohedral symmetry of template-free AlPO-34 (space group $R\bar{3}$) to triclinic (space group $P\bar{1}$). The two template molecules within one *cha* cage are related by an inversion center, and the same is true for the top and bottom faces of the *d6r* units. The first of these fluoro-AlPOs contains morpholinium cations ($C_4H_{10}NO^+$) as template molecules (AlPO-CHA_morph). Its structure was determined by means of synchrotron diffraction using a microcrystal (Harding and Kariuki 1994), and its *P*-dependent behavior was studied up to pressures of 6 GPa (Leardini et al. 2012). A fluoro-AlPO containing pyridinium cations ($C_5H_6N^+$) was prepared by Oliver et al. (AlPO-CHA_pyr, dubbed UT-6 in the original work), and its structure was determined using single-crystal X-ray diffraction (Oliver et al. 1997). An AlPO-CHA system with 1,3-dimethylimidazolium ($C_5H_9N_2^+$) cations in the pores (AlPO-CHA_DMI, dubbed SIZ-10 in the original work), obtained via a ionothermal route, was reported by Parnham & Morris, who determined the structure with synchrotron diffraction using a single crystal

(Parnham and Morris 2006). Finally, a very recent addition to this group of fluoroaluminophosphates is due to Lee et al., who synthesized a chabazite-type AlPO in the presence of 1,2,3-trimethylimidazolium ($(C_6H_{11}N_2^+)$, AlPO-CHA_TMI) (Lee et al. 2016). The structure was determined from powder X-ray diffraction, using a combination of direct methods and Rietveld refinement. While there are no hydrogen bonds in AlPO-CHA_DMI and AlPO-CHA_TMI, the template molecules in AlPO-CHA_morph and AlPO-CHA_pyr are hydrogen-bonded to two/one framework oxygen atoms through their -NH_2/-NH groups.

Prior to the DFT calculations, a water molecule with low occupancy (0.15) was deleted from the structure of AlPO-CHA_pyr. Furthermore, hydrogen atoms were added to the TMI template in AlPO-CHA_TMI, as the H positions had not been determined experimentally in this case. For AlPO-CHA_morph and AlPO-CHA_DMI, the settings of the experimental structures were changed in a way that $\alpha \approx$ 86-87 deg, $\beta \approx$ 77 deg, and $\gamma \approx$ 89 deg in order to make them consistent with the setting used for the other two template-containing AlPOs. In this setting, the four-rings associated with the fluoride anions connect neighboring *d6r* units along the crystallographic *a*-direction (Fig. 1). All experimental lattice parameters are given in Table 1, and the four systems are visualized in Fig. 2.

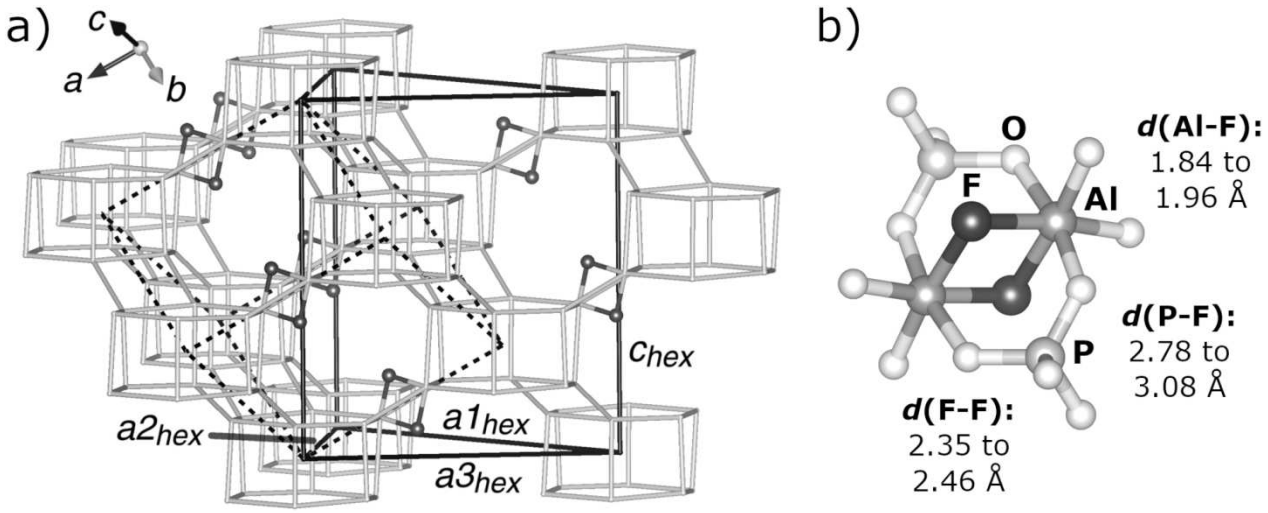

Fig. 1 a) Visualization of the CHA-type fluoroaluminophosphate framework. Template molecules and framework oxygen atoms are omitted for clarity. Dotted lines represent the triclinic axis system, whereas solid lines represent the pseudo-hexagonal axis system (see below). b) "Bridging" arrangement of fluoride anions including the range of Al-F, P-F, and F-F distances found in the experimental structures (Table 1). All structure figures were prepared using VESTA 3 (Momma and Izumi 2011)

Table 1 Experimental lattice parameters and measurement temperatures T_{meas} for AlPO-CHA systems

	AlPO-CHA_morph	AlPO-CHA_pyr	AlPO-CHA_DMI	AlPO-CHA_TMI
T_{meas} / K	293	293	150	293
a / Å	9.162	9.118	9.230	9.228
b / Å	9.183	9.161	9.074	9.286
c / Å	9.333	9.335	9.309	9.379
α / deg	86.24	85.98	87.34	85.21
β / deg	77.43	77.45	76.45	77.31
γ / deg	88.45	89.01	89.39	89.35
V / Å^3	764.7	759.2	757.1	781.3

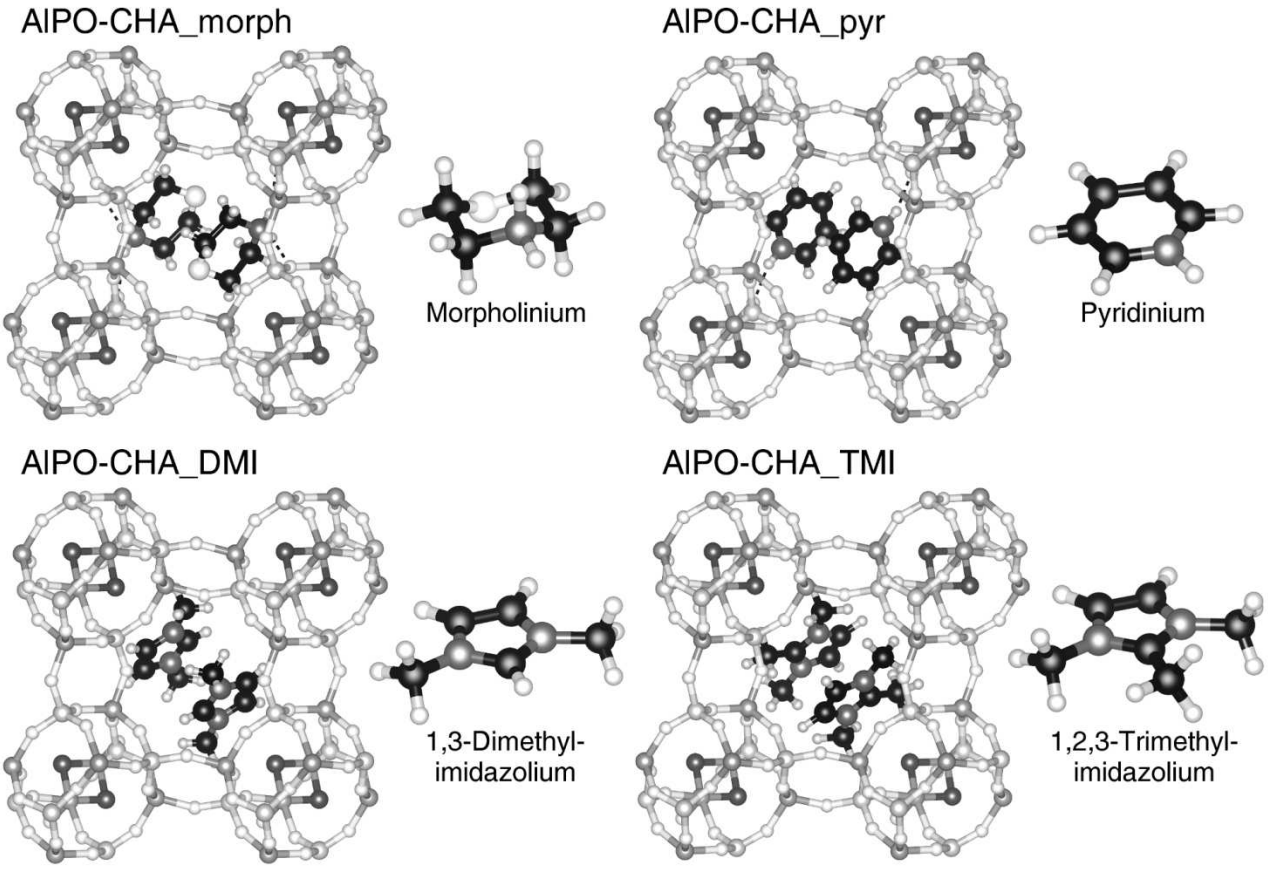

Fig. 2 Visualization of AlPO-CHA systems studied in this work

Details of DFT calculations

All calculations were performed using the CASTEP code (version 7), which employs a combination of plane waves and pseudopotentials (Clark et al. 2005). The calculations used on-the-fly generated ultrasoft pseudopotentials and a plane wave energy cutoff of 800 eV. A 2×2×2 Monkhorst-Pack grid of *k*-points was used to sample the first Brillouin zone. In the initial validation calculations, a total of six different approaches based on the generalized gradient approximation (GGA) were tested: On the one hand, the PBE and PBEsol functionals without dispersion correction were used (Perdew et al. 1996; Perdew et al. 2008). On the other hand, these two functionals were combined with the D2 dispersion correction scheme proposed by Grimme (Grimme 2006; Csonka et al. 2008), and with the TS dispersion correction scheme devised by Tkatchenko and Scheffler (Tkatchenko and Scheffler 2009; Al-Saidi et al. 2012). In all cases, the structures were fully optimized using a BFGS algorithm, including lattice parameters and all atomic coordinates. Optimizations for non-zero hydrostatic pressure conditions were performed by setting the on-diagonal elements of the external pressure tensor to the desired value. Example input keywords for CASTEP are provided as part of the electronic supplementary material.

Results

Method validation

A well-known issue with DFT calculations is the dependence of the results on the choice of the exchange-correlation functional, and on the inclusion (or omission) of a correction term to include long-range dispersion interactions (Perdew et al. 2009; Tran et al. 2016; Mardirossian and Head-Gordon 2017). As our previous work on neutral-framework zeotypes and on water-containing

AlPOs and SAPOs has shown that dispersion-corrected variants of standard GGA functionals perform well for structural parameters, lattice energies, and host-guest interactions energies (Fischer 2015; Fischer 2016; Fischer et al. 2016; Fischer and Angel 2017), the present work concentrates on the same set of functionals, namely the PBE and PBEsol functionals and two dispersion-corrected variants of each. To evaluate the agreement of DFT results with experimental data, the analysis focussed on a) unit cell volumes and b) template-template distances, framework-template distances, and framework-template angles of all four AlPO-CHA systems, and c) the bulk modulus of AlPO-CHA_morph. An analysis of the individual lattice parameters, rather than unit cell volumes, was not found to alter the conclusions regarding the best-performing functional, and is therefore not presented here (the full set of DFT-calculated lattice parameters is supplied in the supplementary material). With regard to T-O bond distances, we have shown in previous benchmarking studies that PBE-based approaches (with or without dispersion correction) lead to a moderate overestimation of the Al-O bond distances, but reproduce P-O distances rather accurately (Fischer et al. 2016). PBEsol-based approaches perform better for Al-O bond lengths, but underestimate P-O distances (Fischer and Angel 2017). Overall, the description of intra-framework bonds and angles is rather similar for all approaches.

When comparing the unit cell volumes obtained from DFT calculations to experimental data, there is a systematic difference because the DFT results correspond to the equilibrium volume at absolute zero, whereas experimental measurements are (obviously) performed at finite temperature. The reference structures used in the present work were obtained at room temperature (RT) or lower temperatures (see Table 1). On the basis of a large collection of data for zeolites and zeotypes, it can be concluded that volume changes between RT and 0 K are typically on the order of 1% or less (Leardini et al. 2015). For the specific case of template-free AlPO-34, Amri and Walton observed a volume change (negative thermal expansion) of about 0.5% between room temperature and 100 K (Amri and Walton 2009). Assuming that template-containing AlPO-CHA systems show a similar

behavior, it can be expected that the unit cell volumes at RT and at 0 K will differ only by a few Å^3. The unit cell volumes obtained from the DFT calculations are shown in Fig. 3, together with experimental data, and the mean of absolute errors (MAE) and mean of signed errors (MSE) of the different DFT approaches are compiled in Table 2. While PBE systematically overestimates the volumes (a well-documented characteristic of this functional (Tran et al. 2016)), all dispersion-corrected functionals underestimate them, by a rather small amount in the case of PBE-D2/-TS (MSE ≈ -5 Å^3), and much more significantly for PBEsol-D2/-TS (MSE ≈ -15 Å^3). The rather poor performance of the latter functionals is somewhat surprising, as they were found to give excellent results for template-free CHA-type AlPO-34, where the calculated volumes of the unit cell (in rhombohedral setting) fall within 2 Å^3 of the experimental value (Fischer and Angel 2017). Of the three functionals delivering a small MAE of ~5 Å^3, PBE-TS is the only one that gives the correct volume ordering of *V*(AlPO-CHA_DMI) < *V*(AlPO-CHA_pyr) < *V*(AlPO-CHA_morph) << *V*(AlPO-CHA_TMI).

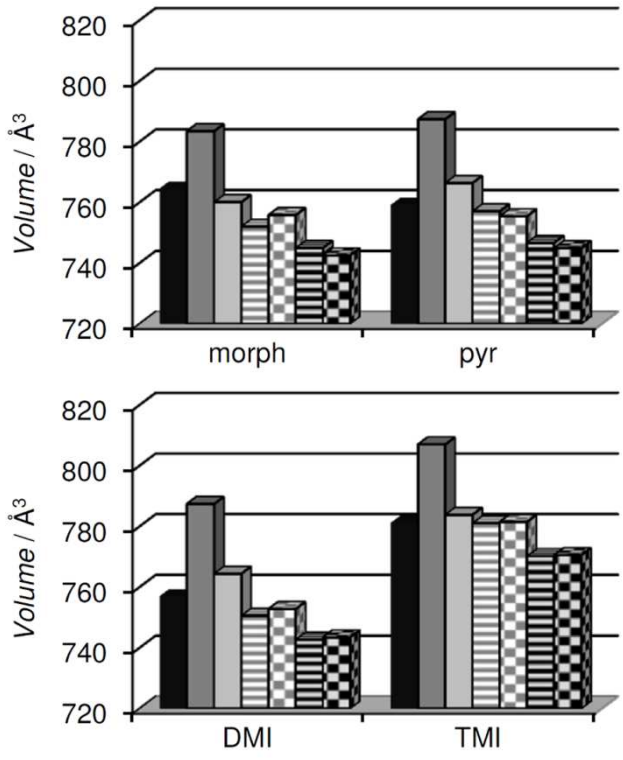

Fig. 3 Unit cell volumes. Black columns represent experimental volumes, remaining columns represent DFT-calculated values obtained with different functionals, from left to right: PBE, PBEsol, PBE-D2, PBE-TS, PBEsol-D2, PBEsol-TS

Table 2 Mean of absolute errors and mean of signed errors in unit cell volumes

	MAE / Å^3	MSE / Å^3
PBE	25.7	25.7
PBEsol	5.4	3.1
PBE-D2	5.4	-5.3
PBE-TS	4.3	-4.2
PBEsol-D2	14.4	-14.4
PBEsol-TS	15.2	-15.2

Fig. 4 shows how the template-template *d*(templ-templ) and framework-template distances *d*(*d6r*-templ) as well as framework-template angles *ω*(*d6r*-templ) were measured. Values of *d*(templ-templ), the distance between the ring centers of two template molecules within one *cha* cage, are compiled in Table 3. For this quantity, PBE performs best, with all values but one agreeing with experiment to within 0.1 Å, whereas PBEsol, and, even more so, dispersion-corrected approaches underestimate *d*(templ-templ), in some instances by more than 0.2 Å. Overall, the trend in template-template distances closely follows that observed above for the unit cell volumes, indicating that the overestimation of template-template interactions might be responsible for the underestimation of unit cell volumes by dispersion-corrected DFT methods. For *d*(*d6r*-templ), the distance between the center of one six-ring of the *d6r* unit and the center of the closest template molecule, agreement between DFT and experiment is fairly good for all functionals, with PBE-TS giving the smallest deviations (Table 3). Finally, the angle *ω*(*d6r*-templ) was measured between the planes constituted by the ring atoms of the template and by the T atoms of the nearest six-ring. We may note that the DMI and TMI molecules are oriented essentially parallel to the six-ring, whereas morpholinium and

pyridinium have an oblique orientation, with ω(*d6r*-templ) = 23.5 deg and 28.9 deg, respectively. For this quantity, all approaches perform similarly well for three of the four AlPOs. The exception is AlPO-CHA_morph, where PBE, PBEsol, and PBEsol-D2 give angles that are rather close to the experimental value, whereas the other three functionals result in a considerably smaller angle, i.e. a less oblique orientation of the template with respect to the *d6r* unit.

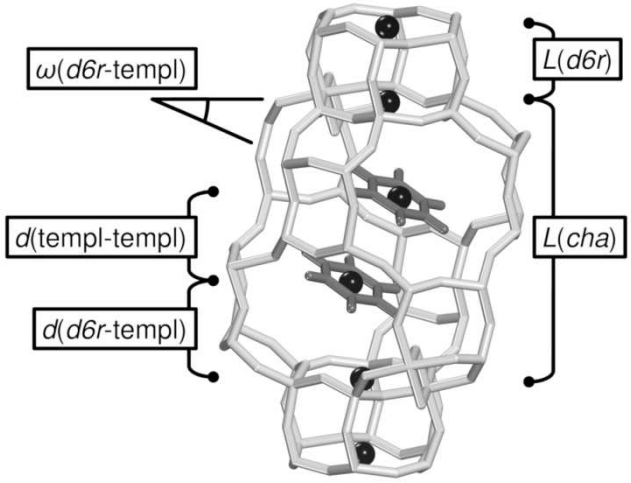

Fig. 4 Schematic visualization of important distances and angles evaluated in this study. Black spheres mark the centers of template molecules and six-rings

Table 3 Template-template distances, framework-template distances, and framework-template angles. Values shown in bold agree with experiment to within 0.1 Å / 2.5 deg, whereas values shown in italics deviate by at least 0.2 Å / 5 deg

	Exp	PBE	PBEsol	PBE-D2	PBE-TS	PBEsol-D2	PBESol-TS
(1) *d*(templ-templ) / Å							
AlPO-CHA_morph	4.19	**4.10**	4.07	*3.95*	4.05	*3.99*	*3.94*
AlPO-CHA_pyr	4.03	**3.95**	3.88	3.87	*3.78*	3.89	3.87
AlPO-CHA_DMI	3.77	**3.87**	**3.76**	3.59	**3.68**	**3.68**	3.66
AlPO-CHA_TMI	3.77	**3.78**	3.59	*3.48*	**3.69**	3.61	3.63
(2) *d*(*d6r*-templ) / Å							

AlPO-CHA_morph	3.81	**3.91**	**3.79**	3.70	**3.79**	**3.74**	**3.76**
AlPO-CHA_pyr	3.93	4.10	4.04	**3.85**	**3.88**	3.79	3.77
AlPO-CHA_DMI	3.79	**3.87**	**3.86**	**3.74**	**3.73**	**3.73**	**3.74**
AlPO-CHA_TMI	3.93	**4.02**	4.04	4.05	**3.92**	**3.95**	**3.95**
(3) ω(*d6r*-templ) / deg							
AlPO-CHA_morph	23.5	**25.6**	**25.3**	*16.9*	*14.3*	**21.4**	*17.0*
AlPO-CHA_pyr	28.9	31.7	32.1	**29.8**	25.1	26.0	24.9
AlPO-CHA_DMI	2.4	**4.5**	**4.2**	**4.6**	5.5	**4.1**	**3.2**
AlPO-CHA_TMI	3.0	**4.9**	7.6	7.6	**3.4**	5.6	5.8

In their experimental study of AlPO-CHA_morph under pressure, Leardini et al. employed a second-order Birch-Murnaghan equation of state to determine the bulk modulus of AlPO-CHA_morph, using the unit cell volumes at pressures between 0.4 and 3.1 GPa (Leardini et al. 2012). They obtained a bulk modulus K_0 of 54(3) GPa, and a volume at zero pressure of 755(1) Å^3. To predict the bulk modulus computationally, DFT optimizations were performed at pressures from 0.5 to 3.0 GPa, with a spacing of 0.5 GPa between the datapoints. From the unit cell volumes, the bulk modulus was calculated using the same equation as in the experimental study, and the results are shown in Table 4 (individual lattice parameters obtained with the different functionals are given in the supplementary material). It is worth noting that there appears to be no systematic difference between dispersion-corrected and uncorrected approaches, with four of the six methods giving an almost identical bulk modulus of ~40 GPa. Use of PBEsol results in a slightly smaller value, but PBE-TS gives the best prediction, with the calculated K_0 of 46 GPa being only 15% smaller than the experimental bulk modulus. Given the experimental uncertainty, this deviation appears acceptable. Overall, PBE-TS can be judged to be the best among the tested approaches, in the light of the good prediction of unit cell volumes, framework-template distances, and the bulk modulus of AlPO-CHA_morph. Nevertheless, it has to be conceded that there remains space for further improvement, especially in the view of the rather large deviations in template-template distances.

Table 4 Bulk moduli K_0 and zero-pressure unit cell volumes V_0 of AlPO-CHA_morph obtained from a second-order Birch-Murnaghan equation of state. For the DFT-computed values, all errors in K_0 and V_0 are smaller than 1 GPa and 1 Å^3, respectively

	K_0 / GPa	V_0 / Å^3
Exp	54(3)	755(1)
PBE	40	783
PBEsol	37	761
PBE-D2	40	752
PBE-TS	46	756
PBEsol-D2	40	746
PBEsol-TS	41	744

Pressure-dependent behavior of AlPO-CHA_morph

In the experimental in-situ study of AlPO-CHA_morph at pressures up to 6 GPa, a refinement of the atomic coordinates at non-ambient conditions was not possible, and only the lattice parameters were refined, using a structure model obtained at 0 GPa (Leardini et al. 2012). In the present work, full DFT optimizations of the structure were performed for pressures from 0 to 5 GPa, so that various other structural parameters in addition to the lattice parameters can be analyzed. Prior to this analysis, we briefly review the experimentally observed evolution. For this discussion, the setting of the structure was changed to conform to that used in the present study, which is why the lattice parameters are labelled differently than in Leardini's work.

The evolution of the normalized experimental lattice parameters is shown in Fig. 5. In the low-pressure regime up to 0.4 GPa, an unusually large volume decrease from 763 Å^3 to 749 Å^3 occurs, with the *b*-axis showing the most pronounced reduction. Between 0.4 and 3.1 GPa, a regular volume contraction by roughly 12 Å^3 per GPa is observed, with *b*, *c*, and β decreasing most prominently. A marked structural change occurs between 3.1 GPa and 3.9 GPa. While the *a*-axis contracts significantly, *b* and *c* remain almost constant. The angles α and β increase sharply, and γ decreases. Upon further pressure increase, contraction of *a* and increase of α continue. The

structural change – which we refer to as "transition" in the following due to the marked discontinuity – is associated with only a modest reduction in volume, and the slope of the volume change decreases gradually above 3.1 GPa. However, it has to be noted that silicone oil, the pressure-transmitting medium, does not behave as an ideal hydrostatic medium at pressures above ~1.0 GPa (Angel et al. 2007). Therefore, as mentioned by Leardini et al., it cannot be ruled out that the observation of a decreased compressibility at pressures above 3 GPa is caused by a non-hydrostatic behavior of the *P*-transmitting medium.

When comparing the evolution of the volume obtained from the PBE-TS calculations (Fig. 5) to experimental data, both common features and discrepancies are apparent. First, the initial volume contraction below 0.5 GPa is not present in the calculations. Instead, there is a linear volume decrease by about 14 $Å^3$ per GPa in the range from 0 to 4 GPa (note that the larger compressibility corresponds to a smaller bulk modulus, as calculated above). Between 4 and 4.5 GPa, i.e. about 1 GPa above the experimental transition pressure, a sharp drop in volume by about 5% (approx. 40 $Å^3$) occurs. While this volume decrease is at variance with the experimental findings, we may still note that the qualitative observation of a transition in this pressure range is correctly reproduced, and that the quantitative experimental findings may be influenced by artefacts arising from non-hydrostatic behavior of the pressure-transmitting medium. From the computational viewpoint, it needs to be considered that the PBE-TS functional tends to overestimate the mutual attraction between template molecules, resulting in the too short template-template distances discussed above. This might also cause an overestimation of the volume contraction associated with the structural transition. For the individual lattice parameters, the evolution up 3 GPa agrees reasonably well with experiment. Most of the changes in lattice parameters at the transition are reproduced qualitatively (e.g. for *a* and the three angles), however, the calculations predict a sharp drop in *c* that is not seen experimentally.

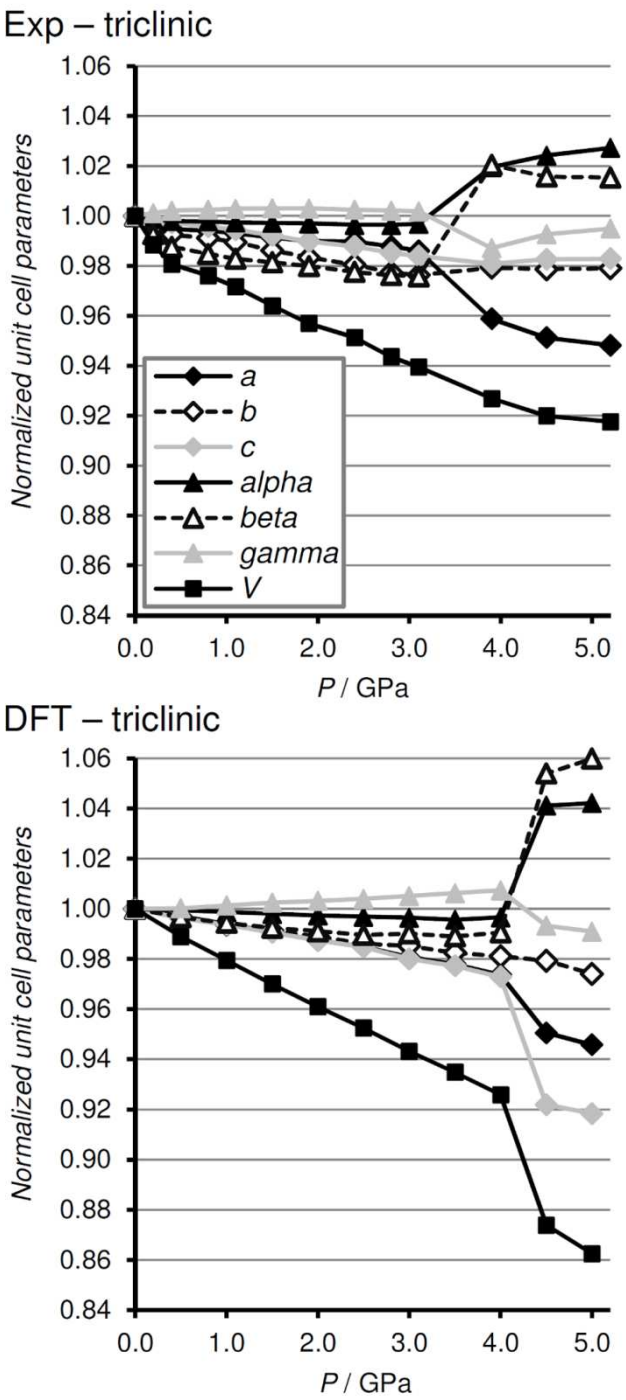

Fig. 5 Evolution of normalized triclinic lattice parameters of AlPO-CHA_morph with pressure

In the hexagonal setting of the chabazite structure, changes in lattice parameters can be easily interpreted as changes in the dimension of the *cha* cage (at least when it is assumed that the *d6r* building units are essentially rigid entities, an assumption we will revisit later): A decrease/increase of the *c*-axis corresponds to a contraction/elongation of the long axis of the cage, and changes in *a*

correspond to a deformation perpendicular to this axis, i.e. changes in the width of the cage. For the triclinic lattice, such a straightforward interpretation is not possible due to the oblique orientation of the coordinate system with respect to the main axes of the cage. However, as already discussed by Leardini et al., it is possible to calculate pseudo-hexagonal lattice parameters that are oriented along the cage axis (c_{hex}) and (approximately) perpendicular to it ($a1_{hex}$, $a2_{hex}$, $a3_{hex}$ – see Fig. 1). In the pressure range up to 3.1 GPa, Leardini et al. observed a contraction of all pseudo-hexagonal lattice parameters, with c_{hex} decreasing most prominently (by about 3%). When the transition occurs, c_{hex} increases by about 4%, whereas all three a_{hex} parameters decrease by 2% to 4%.

The triclinic lattice parameters obtained in the present work were also converted to pseudo-hexagonal parameters, using the following relations:

$$\vec{c}_{hex} = \vec{a}_{tric} + \vec{b}_{tric} - \vec{c}_{tric}$$

$$\vec{a1}_{hex} = \vec{a}_{tric} - \vec{b}_{tric}$$

$$\vec{a2}_{hex} = \vec{b}_{tric} + \vec{c}_{tric}$$

$$\vec{a3}_{hex} = \vec{a}_{tric} + \vec{c}_{tric}$$

Fig. 6 shows the evolution of the pseudo-hexagonal lattice parameters, both from experiment (recalculated from the triclinic lattice parameters reported by Leardini et al.) and from the PBE-TS calculations. The evolution of c_{hex} is reproduced essentially quantitatively, both with regard to the decrease up to the structural transition and the sudden increase associated with the transition. While the deviations for the three a_{hex} parameters are larger, the qualitative behavior is still in good accordance with experiment.

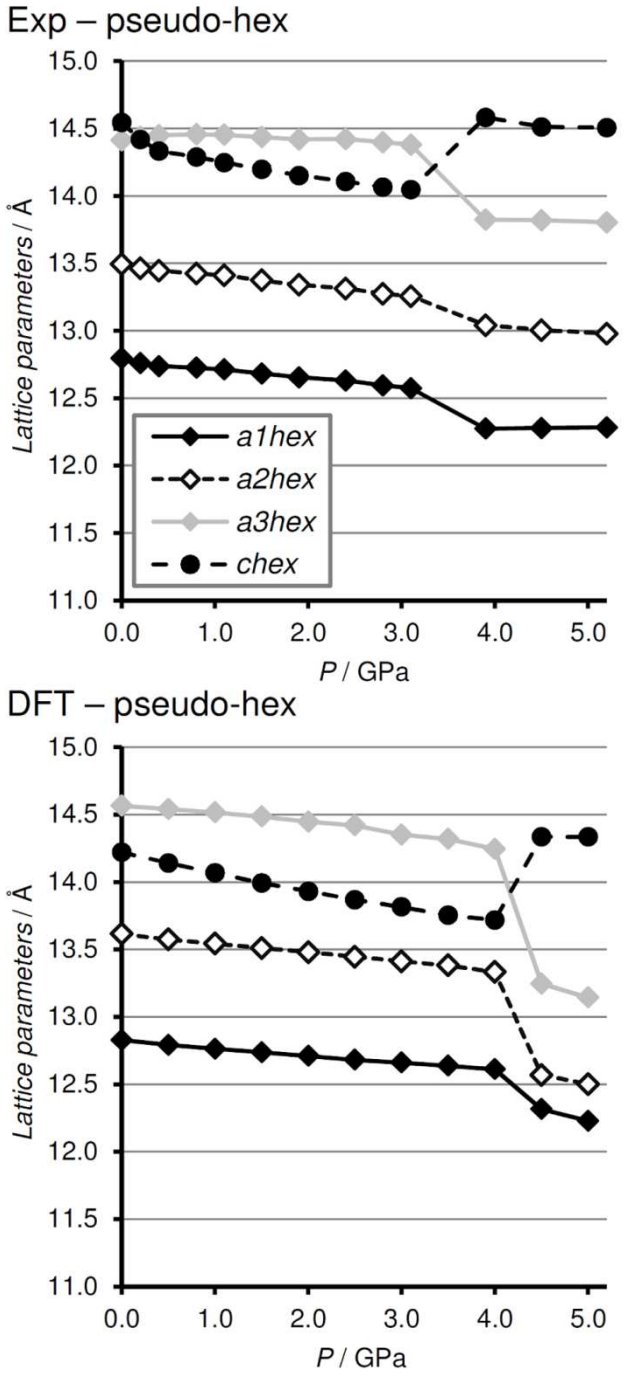

Fig. 6 Evolution of pseudo-hexagonal lattice parameters of AlPO-CHA_morph with pressure

In the discussion of their experimental findings, Leardini et al. hypothesized that the transition at a pressure of 3.1 GPa is associated with an increase in thickness of the *d6r* units (explaining the sudden increase in c_{hex}) and possibly also a reorientation of the template molecules. However, their

atomic-level interpretation remained tentative due to the lack of structural refinements for non-ambient conditions. In the present work, the following structural parameters were analyzed in order to assess the structural changes:

a) The template-template distance *d*(templ-templ), the framework-template distance *d*(*d6r*-templ), and the framework-template angle *ω*(*d6r*-templ), all of which were defined above

b) The length of the long axis of the *cha* cage *L*(*cha*), measured between the centers of six-rings constituting the top and bottom of the cage, and the thickness of a single *d6r* unit *L*(*d6r*), measured between the centers of the two constituent six-rings (Fig. 4)

c) The hydrogen bond distances between H atoms of the NH_2 group of morpholinium and framework oxygen atoms: In the 0 GPa structure, there is one short hydrogen bond (H9···O9), with a length of 1.69 Å, and a rather long hydrogen bond measuring 2.10 Å (H10···O2)

d) The average Al-O-P angle

The evolution of these structural parameters with pressure is visualized in the supplementary material, which also contains structure figures including atom labels.

Fig. 7 visualizes a single *cha* cage of AlPO-CHA_morph at pressures of 0 GPa, 4.0 GPa, and 4.5 GPa. Up to a pressure of 4 GPa, all structural parameters decrease essentially monotonically, the only exception being the H9···O9 hydrogen bond, which retains a more or less constant length. While the long axis of the *cha* cage *L*(cha) decreases by ~0.46 Å, the width of the *d6r* units *L*(*d6r*) shows only a marginal change. The decrease of the *ω*(*d6r*-templ) angle indicates that the morpholinium cations assume a "more parallel" orientation of the template with respect to the *d6r* units, a plausible evolution when considering that the compression of the cage along *c* leaves less space for an oblique orientation. When increasing the pressure from 4 to 4.5 GPa, almost all parameters exhibit a marked change: To start with, *L*(cha) expands from 10.65 Å to 11.36 Å, whereas *L*(*d6r*) decreases from 3.09 Å to 3.00 Å. Moreover, a pronounced increase of framework-

template and template-template distances goes hand-in-hand with a jump of the ω(*d6r*-templ) angle from 8.5 deg to 17.0 deg, i.e. the template reorients within the *cha* cage. The reorientation of the template is also evidenced in the evolution of the hydrogen bond distances: While *d*(H10···O2) changes only slightly, H9 moves away from the framework oxygen atom O9, with *d*(H9···O9) increasing from 1.69 Å to 2.42 Å, and forms a new, shorter hydrogen bond with O11, with *d*(H9···O11) = 2.15 Å (Fig. 8). Another deformation that is associated with the transition between 4 and 4.5 GPa is a "squashing" of the *d6r* units, which is also well visible in Fig. 8: The oxygen-oxygen distances measured across a single six-ring, which fall between 4.9 and 5.3 Å at 0 GPa, decrease only slightly up to 4 GPa. At 4.5 GPa, however, the six-rings become strongly elliptically distorted, with one short oxygen-oxygen distance of 3.36 Å and two long ones in the range of 5.4 to 5.5 Å. The squashing of the *d6r* units is also reflected in a pronounced reduction of the Al-O-P angles between 4 and 4.5 GPa. The average angle decreases from 136.4 to 131.6 deg, and some individual angles decrease by up to 20 deg.

Altogether, the calculations allow us to explain the observed discontinuity in the lattice parameters – for which the calculations largely match the experimentally observed evolution – as being due to the following structural changes: In the framework, the application of pressure leads to an increase in ellipticity of both the *cha* cages and the *d6r* building units, which manifest in an expansion along the pseudo-hexagonal c_{hex} axis and a concurrent contraction of the a_{hex} parameters. Additionally, a reorientation of the template occurs, and the template changes its hydrogen bonding pattern. Clearly, the framework-template interactions will have a certain impact on the response of the inorganic framework to pressure, but it is impossible to quantify to what extent the template influences the overall behavior. It is thus very interesting to assess how the nature of the template affects the pressure-dependent behavior in other CHA-type fluoroaluminophosphates that have not yet been studied experimentally, such as AlPO-CHA_pyr, AlPO-CHA_DMI, and AlPO-CHA_TMI.

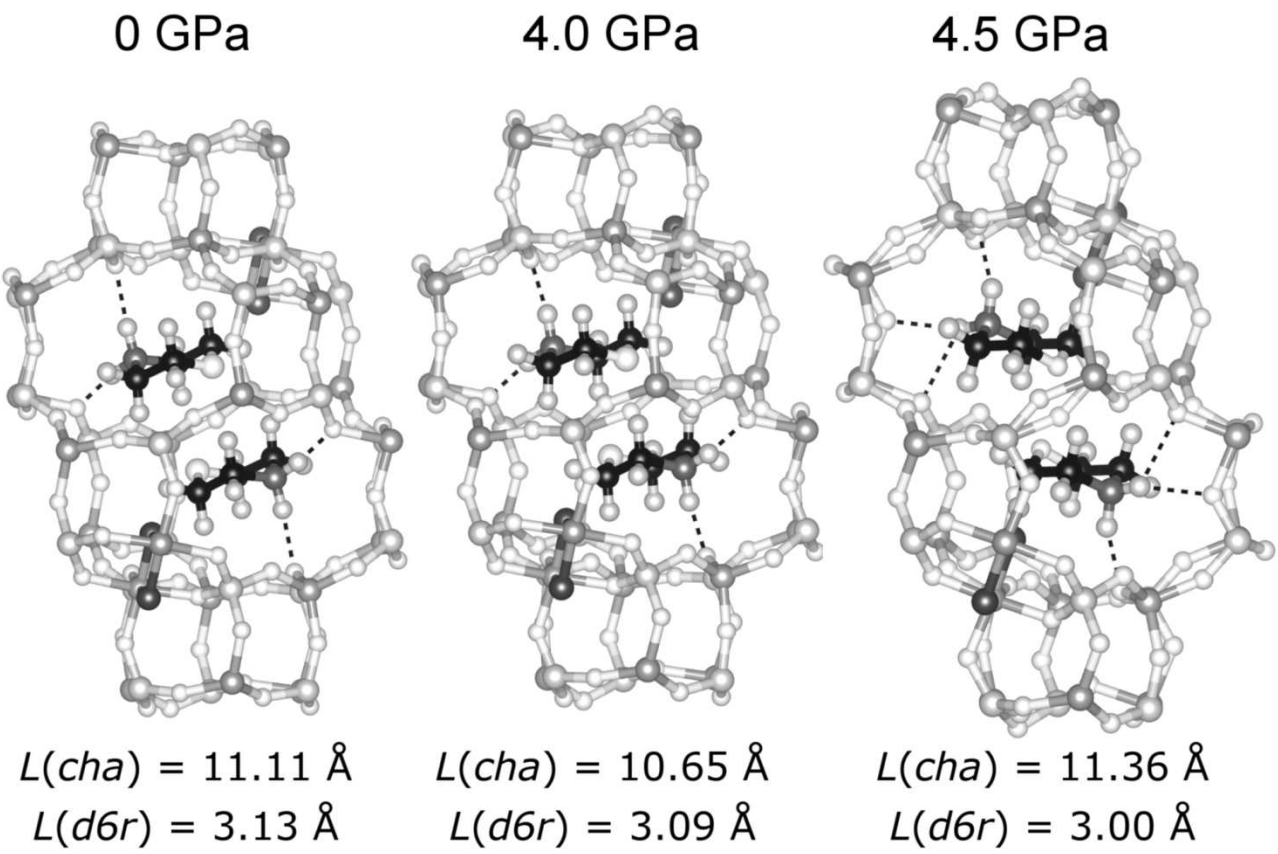

Fig. 7 Visualization of a *cha* cage of AlPO-CHA_morph at three different pressures

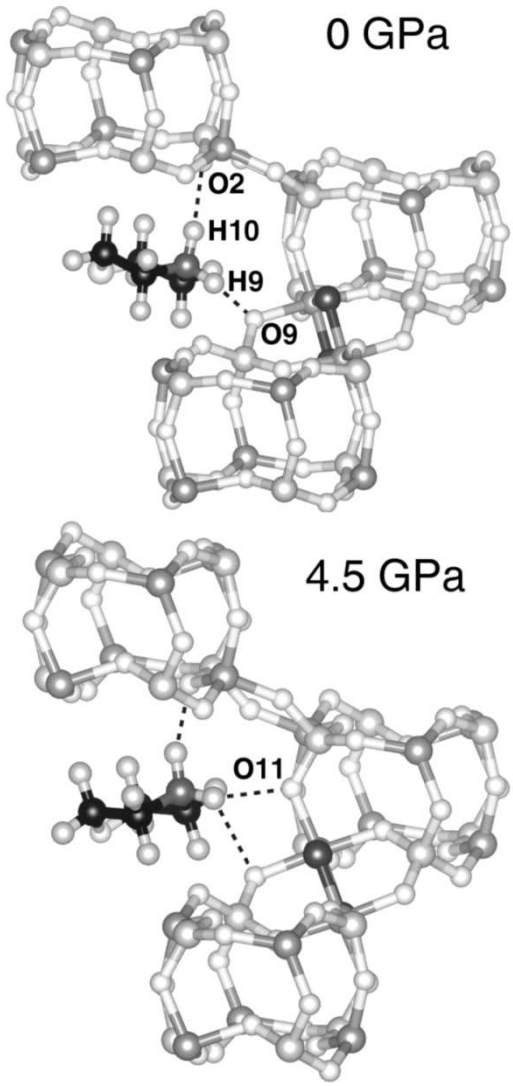

Fig. 8 Template environment in AlPO-CHA_morph at two different pressures

Pressure-dependent behavior of other template-containing AlPOs

The evolution of the unit cell volume as a function of pressure is shown for all AlPO-CHA systems in Fig. 9. AlPO-CHA_pyr exhibits a rather steep volume decrease of about 29 $Å^3$ per GPa in a pressure range from 0 to 2.5 GPa. From 3 GPa onwards, the compressibility decreases, but, unlike for AlPO-CHA_morph, there is no marked discontinuity. Calculation of the bulk modulus in the pressure range up to 2.5 GPa (Table 5) delivers a value of only 19 GPa, much lower than for AlPO-CHA_morph. An inspection of the pseudo-hexagonal lattice parameters reveals that the

compression happens predominantly along c_{hex}, which decreases by 11% (from 14.12 to 12.50 Å) in the pressure range studied. Consequently, the length of the *cha* cage *L*(*cha*) decreases by ~1.5 Å, and the eight-ring windows become more and more elliptically distorted (Fig. 10). The template, which assumes a fairly oblique orientation at ambient conditions, with ω(*d6r*-templ) = 25.1 deg, rotates and aligns more or less parallel to the *d6r* unit upon the application of pressure. Interestingly, the *d6r* units also behave qualitatively differently than in AlPO-CHA_morph. Between pressures of 1.5 and 2 GPa, one of the equatorial Al-O-P linkages of the *d6r* unit, the Al3-O4-P1 linkage, inverts: The O4 atom, which points outward at lower pressures as is typical for this building unit, points towards the center of the *d6r* unit at higher pressures (Fig. 10). Despite this deformation in the equatorial plane, the six-rings at the top and bottom of the *d6r* unit are less distorted than in AlPO-CHA_morph.

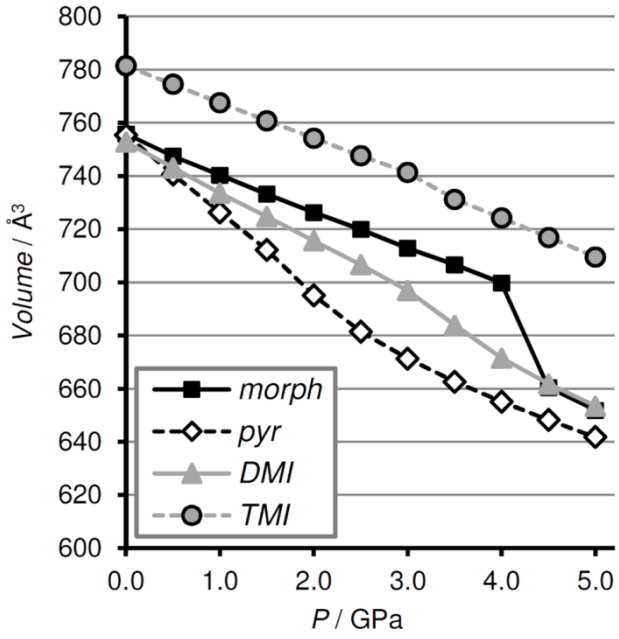

Fig. 9 Evolution of the unit cell volumes with pressure in different AlPO-CHA systems

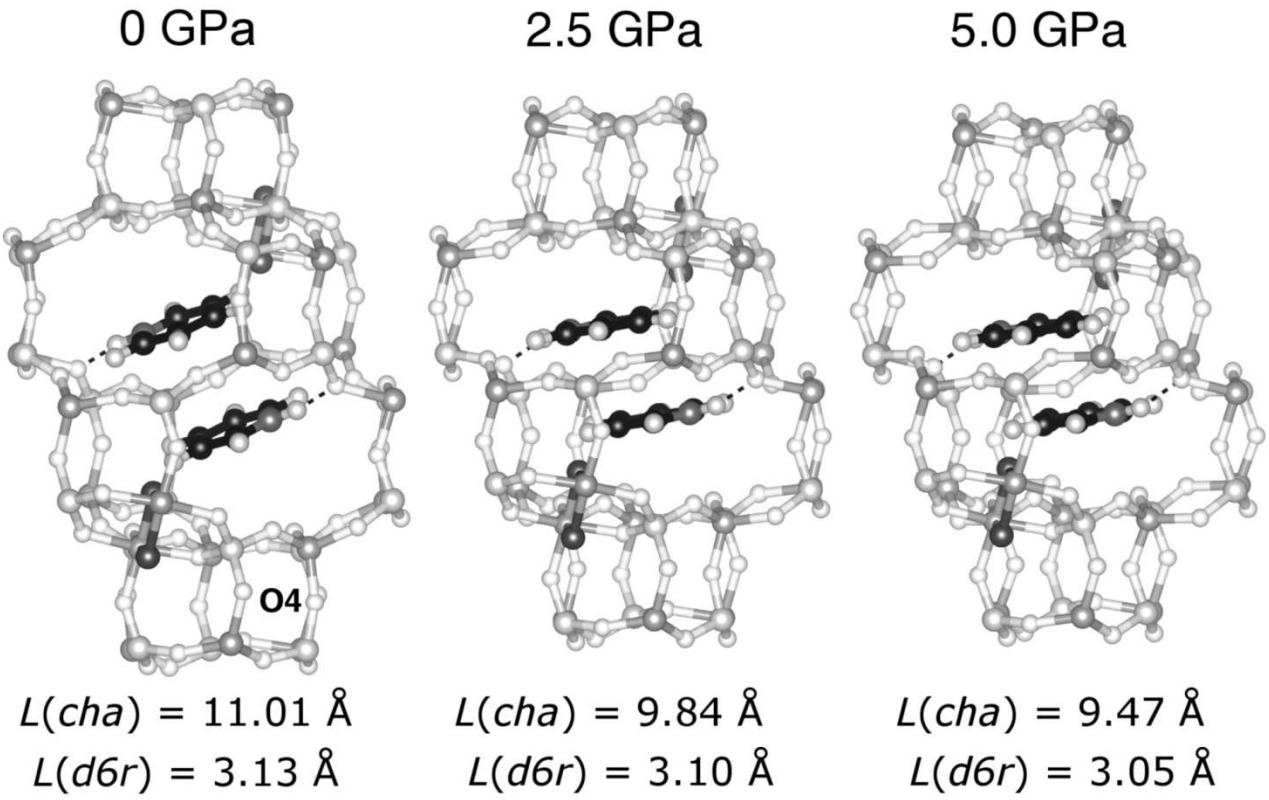

Fig. 10 Visualization of a *cha* cage of AlPO-CHA_pyr at three different pressures

The volume decrease of AlPO-CHA_DMI at pressures up to 3 GPa is intermediate between those of AlPO-CHA_morph and AlPO-CHA_pyr, with a reduction of about 18 $Å^3$ per GPa (bulk modulus: 33 GPa). The compressibility increases slightly between 3 and 4 GPa, but has approximately the same magnitude as in the low-pressure range above 4 GPa. Again, the c_{hex} parameter decreases most prominently, however, the overall contraction of about 8% is smaller than in AlPO-CHA_pyr, and *L*(*cha*) decreases by about 1 Å. Unlike in the systems discussed so far, there is hardly any rotation of the template in AlPO-CHA_DMI: The dimethylimidazolium molecules are oriented almost parallel to the *d6r* unit at ambient conditions, and rotate by less than 2 degrees over the whole pressure range. With the exception of the framework-template angle, the discontinuity that is visible in the volume evolution between 3 and 4 GPa can also be traced in the other structural parameters considered. In particular, the average Al-O-P angle, which amounts to 138.6 deg at 0 GPa, drops

from 135.6 deg at 3.0 GPa to 132.4 GPa at 4.0 GPa. A look at the individual values shows that this is mainly due to a dramatic change in the Al3-O12-P1 angle, an equatorial linkage of the *d6r* unit: This angle amounts to 159 deg at 0 GPa, and increases until it is almost linear at 3.0 GPa. Upon further pressure increase, the linkage inverts as observed above for AlPO-CHA_pyr, i.e. the O12 atom points towards the interior of the *d6r* building unit (Fig. 11). While the pressure at which this inversion occurs differs by about 1.5 GPa between the two systems, the unit cell volume is rather similar, being in the range of ~700 Å^3.

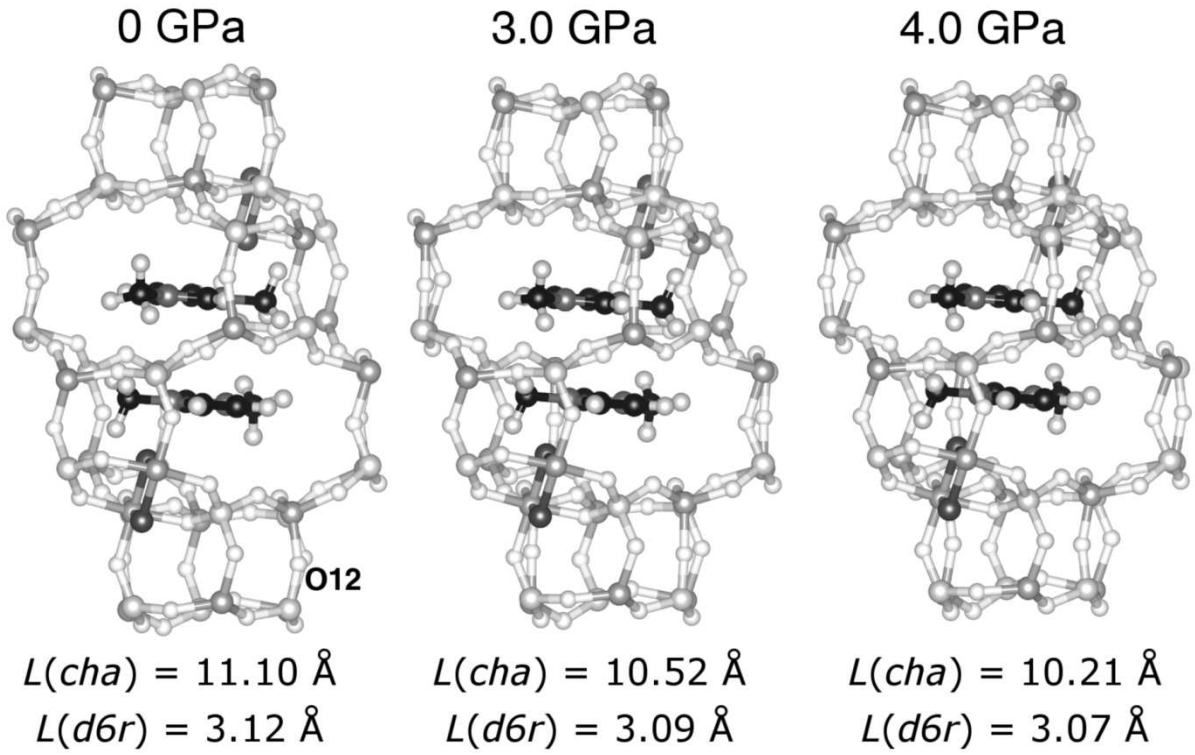

Fig. 11 Visualization of a *cha* cage of AlPO-CHA_DMI at three different pressures

AlPO-CHA_TMI exhibits the shallowest slope of the volume decrease with pressure, with a reduction of the volume by about 13 Å^3 per GPa between 0 and 3 GPa (K_0 = 51 GPa). In this pressure range, all of the investigated structural parameters decrease more or less continuously.

Between 3 and 3.5 GPa, there is a small discontinuity, with a volume reduction by about 10 $Å^3$ between these two pressure points. The discontinuity is also visible in some other structural parameters: For example, the template-template distance increases from 3.59 Å to 3.61 Å, and the framework-template angle, which remains essentially constant up to 3 GPa, increases from 3.3 to 4.4 deg. This indicates that the discontinuity is associated with a slight rearrangement of the template. Above 3.5 GPa, the compressibility is altogether similar to that in the pressure range between 0 and 3 GPa. As is visible in Fig. 12, a rotation of the methyl groups occurs between 3 and 5 GPa, which is probably responsible for the somewhat discontinuous evolution of template-template and framework-template distances as well as ω(*d6r*-templ) in this pressure range. The overall volume reduction between 0 and 5 GPa amounts to 9%, compared to 13% in AlPO-CHA_DMI, 14% in AlPO-CHA_morph, and 15% in AlPO-CHA_pyr. In the pseudo-hexagonal axis system, the largest compression is observed along the c_{hex}-axis (~5%), corresponding to a reduction of the *L*(*cha*) parameter by about 0.7 Å. The relatively high stiffness of AlPO-CHA_TMI is also reflected in a much less pronounced reduction of the average Al-O-P angle, which amounts to ~137 deg at 5 GPa, compared to ~130 deg in the other three systems. There is no inversion of an Al-O-P linkage in the pressure range studied, however, the Al3-O12-P3 angle increases from 158 deg at 0 GPa to 172 deg at a pressure of 5 GPa, so an inversion might take place upon further pressure increase.

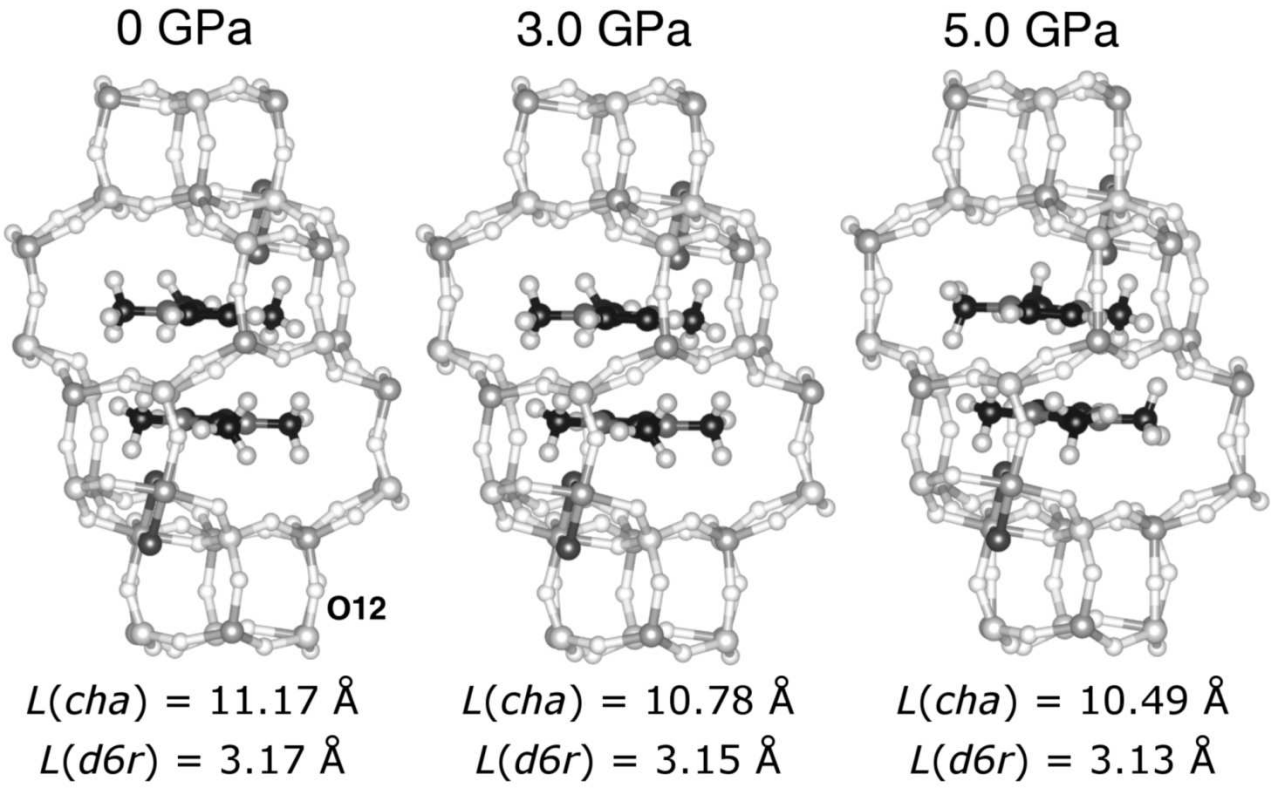

Fig. 12 Visualization of a *cha* cage of AlPO-CHA_TMI at three different pressures

Discussion

In summary, the nature of the template has a significant impact on two different aspects of the elastic behavior of CHA-type AlPOs: Firstly, the bulk modulus in the pressure range up to ~3 GPa, where the unit cell volumes show essentially a linear decrease, varies greatly depending on the template. Secondly, the (non-)occurrence of a structural transition above this pressure is also template-dependent: While AlPO-CHA_morph exhibits a very pronounced structural change, the discontinuities in AlPO-CHA_DMI and AlPO-CHA_TMI are on a much smaller scale. AlPO-CHA_pyr, while being strongly deformed upon the application of pressure, does not show a marked discontinuity, but primarily a flattening of the pressure-volume curve above 2.5 GPa.

In order to analyze the relationship between the "bulkiness" (the molecular volume) of the template molecule and the compressibility in a quantitative fashion, the molecular volumes of the template molecules were calculated using Voronoi-Dirichlet partitioning as implemented in the software TOPOS (Blatov et al. 2014). The molecular volumes are included in Table 5. On the basis of these values, a near-perfect correlation between molecular volume and bulk modulus can be observed for AlPO-CHA_pyr, AlPO-CHA_DMI, and AlPO-CHA_TMI: Since increasing molecular dimensions of the template lead to a more efficient filling of the *cha* cage, the system with the bulkiest template is most resistant to compression. The analysis presented above has also shown that different template molecules exhibit a very different degree of rotation with pressure: The five-membered rings with attached methyl groups, DMI and TMI, are essentially aligned with the *d6r* unit even at ambient conditions. In a very simplified fashion, the *d6r*-template-template-*d6r* sequence within one *cha* cage can be viewed as a stacking of more or less flat disks along the cage axis. Such a stack of disks can accommodate pressure by moving the disks closer together, but not by rotation. The possibility to compress this arrangement along the cage axis is therefore limited, leading to a relatively high stiffness along the c_{hex} axis. In contrast, the pyridinium template assumes a highly tilted orientation at ambient conditions. It can react to pressure by gradually aligning with the *d6r* units. Moreover, the flat aromatic pyridinium template can form somewhat shorter framework-template and template-template contacts than DMI and TMI, consequently allowing the cage to deform to a larger extent.

AlPO-CHA_morph departs from the correlation between molecular volume and bulk modulus: While the dimensions of morpholinium are very similar to those of the DMI molecule, the bulk modulus of AlPO-CHA_morph is 13 GPa higher than that of AlPO-CHA_DMI. Furthermore, we may note that the unit cell volumes of AlPO-CHA_morph and AlPO-CHA_DMI at pressures above 4 GPa are essentially identical, in line with the similar molecular volume of the template, whereas AlPO-CHA_morph has a larger unit cell volume at lower pressures (Fig. 9). This indicates that the

presence of the morpholinium template stabilizes a lower-density arrangement. Tentatively, we can attribute this to the presence of hydrogen bonds on the one hand, and to the non-planarity of the morpholinium molecule on the other hand: Where the aromatic pyridinium, DMI, and TMI molecules can form fairly short template-template contacts due to attractive π-stacking interactions, such a close approach of morpholinium molecules is prevented by the non-planarity of the non-aromatic six-ring, where hydrogen atoms that point out of the plane repel each other. As a consequence, the molecular volume of the template can only give a rough guideline to predict its impact on the compressibility, since steric effects, the presence/absence of hydrogen bonds, and other template-template and framework-template interactions also play an important role.

Table 5 Bulk moduli K_0 and unit cell volumes at P = 0 GPa V_0 obtained from a second-order Birch-Murnaghan equation of state and molecular volume V_{templ} of template molecules. The equation of state was fitted for a pressure range from 0 to 2.5 GPa for AlPO-CHA_pyr, and from 0 to 3 GPa for all other systems

	K_0 / GPa	V_0 / Å^3	V_{templ} / Å^3
AlPO-CHA_morph	46(1)	756(1)	152
AlPO-CHA_pyr	19(1)	759(3)	141
AlPO-CHA_DMI	33(1)	754(1)	156
AlPO-CHA_TMI	51(1)	782(1)	175

This brings us directly to the second point, namely the discontinuities in the compressional behavior above ~3 GPa. The transition in AlPO-CHA_morph, which is associated with a elongation of the *cha* cage, can also be explained with the repulsion between the morpholinium molecules: At a point where pressure cannot be accommodated anymore by further rotation and decrease of the template-template distance, the templates "slip" against each other, assuming a different orientation in the cage and increasing the intermolecular distance (Fig. 7). This rearrangement can only be accommodated through a pronounced change in the cage dimensions. Simply on the basis of the

observations made for AlPO-CHA_morph, one might hypothesize that the occurrence of the transition associated with an abrupt elongation of the *cha* cage is template-independent and will occur when the cage is compressed beyond a certain limit. However, the comparison with AlPO-CHA_pyr shows that this is not the case, as *L*(*cha*) is reduced to a much larger extent without any transition in the latter system. Along the same lines, one can conjecture that the observed "squashing" of the *d6r* unit in AlPO-CHA_morph is a consequence of the cage elongation, rather than vice versa, as such a deformation is not observed in any other AlPO-CHA system under pressure.

For AlPO-CHA_pyr, AlPO-CHA_DMI, and AlPO-CHA_TMI, there is no evidence for a marked structural transition, although certain discontinuities in the volume evolution are observed. These are correlated with minor reorientations of the template molecules that are far less pronounced than in AlPO-CHA_morph. A particularly interesting finding made for AlPO-CHA_pyr and AlPO-CHA_DMI is the inversion of one of the equatorial Al-O-P linkages of the *d6r* building unit. This, together with the occurrence of "squashed" *d6r* units in AlPO-CHA_morph, indicates that this building unit can accommodate pressure through rather pronounced internal deformations, i.e. it does not act as a rigid entity. Experimentally, an increase of the equatorial T-O-T angle of the *d6r* unit has been observed only at low pressures, between 0 and 0.3 GPa in chabazite and between 0 and 1 GPa in levyne, and there has been no evidence for an inversion of the linkage (Gatta et al. 2005; Leardini et al. 2013). However, it has to be noted that these aluminosilicate frameworks consist exclusively of tetrahedral units, whereas the CHA-type fluoroaluminophosphates contain AlO_4F_2 octahedra. As these octahedral units are relatively rigid (which is evidenced, for example, by the near-constant Al-F-Al angle of 99 deg in all systems at all pressures), other parts of the structure will have to deform more strongly in response to applied pressure.

Conclusions

In this contribution, we have presented an in-depth DFT study of the compressional behavior of CHA-type fluoroaluminophosphates containing different template molecules. The initial test of different flavors of DFT with and without dispersion correction showed that the PBE-TS functional reproduces different structural parameters as well as the bulk modulus of AlPO-CHA_morph. Moreover, it also provides a qualitatively correct picture of the lattice parameters' evolution during the structural transition, although it overestimates the transition pressure by about 1 GPa and exaggerates the volume contraction. A similar behavior has been observed in DFT studies of natrolites, where PBE overestimates the pressure at which pressure-induced hydration occurs by about 1 GPa (Kremleva et al. 2013; Kremleva et al. 2014). Altogether, we can expect that the PBE-TS functional is sufficiently reliable for semi-quantitative studies of the *P*-dependent structural evolution of zeolite frameworks, at least up to moderate pressures, but that other, more advanced dispersion-corrected DFT methods may be needed for accurate quantitative predictions.

The computations of the *P*-dependent behavior of the four AlPO-CHA systems showed that the compressibility in the pressure range up to ~3 GPa depends on the molecular volume of the template, but also on the nature of the dominant interactions. Rather more surprisingly, the calculations revealed that the nature of the template also determines whether a structural transition occurs in a pressure range up to 5 GPa, as the marked structural change found for AlPO-CHA_morph is not observed in any other system. The detailed analysis revealed that the transition in AlPO-CHA_morph can be understood as being triggered by the template reorientation. Even among the three systems that do not exhibit a marked transition, some differences in the deformation of the framework are evident, indicating a more subtle influence of the template on the compressional behavior.

After having made detailed computational predictions for several structurally related systems, it would be interesting to perform new experimental in-situ investigations in order to assess to what extent the theoretical predictions reproduce the experimental observations, to analyze where they

deviate, and to trace – where possible – whether deviations are due to failings of the computational approach or due to non-idealities in the experimental conditions. In this spirit, future joint efforts by experimentalists and theoreticians should further enhance our understanding of zeolite frameworks under pressure. Framework-template interactions in zeolites are predominantly important in synthetic materials, where the organic species are used to "direct" the synthesis of a particular topology. However, it should be noted that some minerals, like the feldspathoid tsaregorodtsevite (Sherriff et al. 1997) and natural clathrates like melanophlogite and chibaite (Gies 1983; Momma et al. 2011; Momma 2014), also incorporate organic species in confined spaces. This highlights the significance of such host-guest interactions in a geoscientific context, in addition to their (more obvious) importance in materials science.

Acknowledgments

The author acknowledges funding by the Central Research Development Funds of the University of Bremen and by the Deutsche Forschungsgemeinschaft (DFG, German Research Foundation), project number 389577027 (FI 1800/5-1). The author would like to thank Diego Gatta for helpful discussions, and Gloria Tabacchi and one anonymous reviewer for insightful and encouraging comments.

Electronic supplementary material

Supplementary tables and figures are provided in a separate PDF document. Structures of AlPO-CHA systems at different pressures obtained from DFT optimizations are included as CIF files.

Conflict of Interest

The author declares that he has no conflict of interest.

References

Al-Saidi WA, Voora VK, Jordan KD (2012) An Assessment of the vdW-TS Method for Extended Systems. J Chem Theory Comput 8:1503–1513. https://doi.org/10.1021/ct200618b

Amri M, Walton RI (2009) Negative Thermal Expansion in the Aluminum and Gallium Phosphate Zeotypes with CHA and AEI Structure types. Chem Mater 21:3380–3390. https://doi.org/10.1021/cm901140u

Angel RJ, Bujak M, Zhao J, Gatta GD, Jacobsen SD (2007) Effective hydrostatic limits of pressure media for high-pressure crystallographic studies. J Appl Crystallogr 40:26–32. https://doi.org/10.1107/S0021889806045523

Baerlocher C, McCusker LB, Olson DH (2007) Atlas of Zeolite Framework Types, 6th edn. Elsevier B.V., Amsterdam, NL

Betti C, Fois E, Mazzucato E, Medici C, Quartieri S, Tabacchi G, Vezzalini G, Dmitriev V (2007) Gismondine under HP: Deformation mechanism and re-organization of the extra-framework species. Microporous Mesoporous Mater 103:190–209. https://doi.org/10.1016/j.micromeso.2007.01.051

Blatov VA, Shevchenko AP, Proserpio DM (2014) Applied Topological Analysis of Crystal Structures with the Program Package ToposPro. Cryst Growth Des 14:3576–3586. https://doi.org/10.1021/cg500498k

Clark SJ, Segall MD, Pickard CJ, Hasnip PJ, Probert MIJ, Refson K, Payne MC (2005) First principles methods using CASTEP. Z Kristallogr 220:567–570. https://doi.org/10.1524/zkri.220.5.567.65075

Combariza AF, Gomez DA, Sastre G (2013) Simulating the properties of small pore silica zeolites using interatomic potentials. Chem Soc Rev 42:114–127. https://doi.org/10.1039/c2cs35243e

Corà F, Catlow CRA (2001) Ionicity and framework stability of crystalline aluminophosphates. J Phys Chem B 105:10278–10281. https://doi.org/10.1021/jp0107053

Coudert F-X (2013) Systematic investigation of the mechanical properties of pure silica zeolites: stiffness, anisotropy, and negative linear compressibility. Phys Chem Chem Phys 15:16012–16018. https://doi.org/10.1039/c3cp51817e

Csonka GI, Ruzsinszky A, Perdew JP, Grimme S (2008) Improved description of stereoelectronic effects in hydrocarbons using semilocal density functional theory. J Chem Theory Comput 4:888–891. https://doi.org/10.1021/ct800003n

Fischer M (2015) Water adsorption in SAPO-34: elucidating the role of local heterogeneities and defects using dispersion-corrected DFT calculations. Phys Chem Chem Phys 17:25260–25271. https://doi.org/10.1039/C5CP04189A

Fischer M (2016) Interaction of water with (silico)aluminophosphate zeotypes: a comparative investigation using dispersion-corrected DFT. Phys Chem Chem Phys 18:15738–15750. https://doi.org/10.1039/C6CP02289H

Fischer M, Angel RJ (2017) Accurate structures and energetics of neutral-framework zeotypes from dispersion-corrected DFT calculations. J Chem Phys 146:174111. https://doi.org/10.1063/1.4981528

Fischer M, Evers FO, Formalik F, Olejniczak A (2016) Benchmarking DFT-GGA calculations for the structure optimisation of neutral-framework zeotypes. Theor Chem Acc 135:257. https://doi.org/10.1007/s00214-016-2014-6

Fois E, Gamba A, Medici C, Tabacchi G, Quartieri S, Mazzucato E, Arletti R, Vezzalini G, Dmitriev V (2008) High pressure deformation mechanism of Li-ABW: Synchrotron XRPD study and ab initio molecular dynamics simulations. Microporous Mesoporous Mater 115:267–280. https://doi.org/10.1016/j.micromeso.2008.01.041

Fois E, Gamba A, Tabacchi G, Arletti R, Quartieri S, Vezzalini G (2005) The "template" effect of the extra-framework content on zeolite compression: The case of yugawaralite. Am Mineral 90:28–35. https://doi.org/10.2138/am.2005.1653

Gatta GD, Comodi P, Zanazzi PF, Boffa Ballaran T (2005) Anomalous elastic behavior and high-pressure structural evolution of zeolite levyne. Am Mineral 90:645–652. https://doi.org/10.2138/am.2005.1768

Gatta GD, Lee Y (2014) Zeolites at high pressure: A review. Mineral Mag 78:267–291. https://doi.org/10.1180/minmag.2014.078.2.04

Gatta GD, Lotti P, Tabacchi G (2018) The effect of pressure on open-framework silicates: elastic behaviour and crystal–fluid interaction. Phys Chem Miner 45:115–138. https://doi.org/10.1007/s00269-017-0916-z

Gatta GD, Scheidl KS, Pippinger T, Skála R, Lee Y, Miletich R (2015) High-pressure behavior and crystal–fluid interaction under extreme conditions in paulingite [PAU-topology]. Microporous Mesoporous Mater 206:34–41. https://doi.org/10.1016/j.micromeso.2014.11.031

Gies H (1983) Studies on clathrasils. III. Crystal structure of melanophlogite, a natural clathrate compound of silica. Z Kristallogr - Cryst Mater 164:247-257. https://doi.org/10.1524/zkri.1983.164.3-4.247

Grimme S (2006) Semiempirical GGA-type density functional constructed with a long-range dispersion correction. J Comput Chem 27:1787–1799. https://doi.org/10.1002/jcc.20495

Harding MM, Kariuki BM (1994) Microcrystal structure determination of $AlPO_4$-CHA using synchrotron radiation. Acta Crystallogr C 50:852–854. https://doi.org/10.1107/S0108270194000326

Kremleva A, Vogt T, Rösch N (2013) Monovalent Cation-Exchanged Natrolites and Their Behavior under Pressure. A Computational Study. J Phys Chem C 117:19020–19030. https://doi.org/10.1021/jp406037c

Kremleva A, Vogt T, Rösch N (2014) Potassium-Exchanged Natrolite Under Pressure. Computational Study vs Experiment. J Phys Chem C 118:22030–22039. https://doi.org/10.1021/jp505973r

Leardini L, Quartieri S, Martucci A, Vezzalini G, Dmitriev V (2012) Compressibility of microporous materials with CHA topology: 2. ALPO-34. Z Kristallogr - Cryst Mater 227:514–521. https://doi.org/10.1524/zkri.2012.1477

Leardini L, Quartieri S, Vezzalini G (2010) Compressibility of microporous materials with CHA topology: 1. Natural chabazite and SAPO-34. Microporous Mesoporous Mater 127:219–227. https://doi.org/10.1016/j.micromeso.2009.07.017

Leardini L, Quartieri S, Vezzalini G, Arletti R (2015) Thermal behaviour of siliceous faujasite: Further structural interpretation of negative thermal expansion. Microporous Mesoporous Mater 202:226–233. https://doi.org/10.1016/j.micromeso.2014.10.006

Leardini L, Quartieri S, Vezzalini G, Martucci A, Dmitriev V (2013) Elastic behavior and high pressure-induced phase transition in chabazite: New data from a natural sample from Nova Scotia. Microporous Mesoporous Mater 170:52–61. https://doi.org/10.1016/j.micromeso.2012.11.024

Lee JH, Kim EJ, López-Arbeloa F, Hong SB, Camblor MA (2016) Microporous aluminophosphates synthesized with 1,2,3-trimethylimidazolium and fluoride. Dalton Trans 45:7616–7626. https://doi.org/10.1039/C6DT00734A

Loiseau T, Férey G (2007) Crystalline oxyfluorinated open-framework compounds: Silicates, metal phosphates, metal fluorides and metal-organic frameworks (MOF). J Fluor Chem 128:413-422. https://doi.org/10.1016/j.jfluchem.2006.09.009

Mardirossian N, Head-Gordon M (2017) Thirty years of density functional theory in computational chemistry: An overview and extensive assessment of 200 density functionals. Mol Phys 115:2315–2372. https://doi.org/10.1080/00268976.2017.1333644

Masters AF, Maschmeyer T (2011) Zeolites – From curiosity to cornerstone. Microporous Mesoporous Mater 142:423–438. https://doi.org/10.1016/j.micromeso.2010.12.026

Momma K (2014) Clathrate compounds of silica. J Phys Condens Matter 26:103203. https://doi.org/10.1088/0953-8984/26/10/103203

Momma K, Ikeda T, Nishikubo K, Takahashi N, Honma C, Takada M, Furukawa Y, Nagase T, Kudoh Y (2011) New silica clathrate minerals that are isostructural with natural gas hydrates. Nat Commun 2:196. https://doi.org/10.1038/ncomms1196

Momma K, Izumi F (2011) VESTA 3 for three-dimensional visualization of crystal, volumetric and morphology data. J Appl Crystallogr 44:1272–1276. https://doi.org/10.1107/S0021889811038970

Oliver S, Kuperman A, Lough A, Ozin GA (1997) Synthesis and characterization of a fluorinated anionic aluminophosphate framework UT-6, and its high-temperature dehydrofluorination to $AlPO_4$-CHA. J Mater Chem 7:807–812. https://doi.org/10.1039/a606828f

Parnham ER, Morris RE (2006) 1-Alkyl-3-methyl Imidazolium Bromide Ionic Liquids in the Ionothermal Synthesis of Aluminium Phosphate Molecular Sieves. Chem Mater 18:4882–4887. https://doi.org/10.1021/cm0615929

Passaglia E, Sheppard RA (2001) The Crystal Chemistry of Zeolites. Rev Mineral Geochemistry 45:69–116. https://doi.org/10.2138/rmg.2001.45.2

Perdew J, Ruzsinszky A, Csonka G, Vydrov O, Scuseria G, Constantin L, Zhou X, Burke K (2008) Restoring the Density-Gradient Expansion for Exchange in Solids and Surfaces. Phys Rev Lett 100:136406. https://doi.org/10.1103/PhysRevLett.100.136406

Perdew JP, Burke K, Ernzerhof M (1996) Generalized Gradient Approximation Made Simple. Phys Rev Lett 77:3865–3868. https://doi.org/10.1103/PhysRevLett.77.3865

Perdew JP, Ruzsinszky A, Constantin LA, Sun J, Csonka GI (2009) Some Fundamental Issues in Ground-State Density Functional Theory: A Guide for the Perplexed. J Chem Theory Comput 5:902–908. https://doi.org/10.1021/ct800531s

Sherriff BL, Sokolova E V., Cramer J, Kunath-Fandei G, Jaeger C, Pautov LA (1997) Changes in the crystal structure of tsaregorodtsevite $[N(CH_3)_4][Si_2(Si_{0.5}Al_{.05})O_6]_2$ on heating. Am Mineral 82:405–415. https://doi.org/10.2138/am-1997-3-418

Tkatchenko A, Scheffler M (2009) Accurate Molecular Van Der Waals Interactions from Ground-State Electron Density and Free-Atom Reference Data. Phys Rev Lett 102:73005. https://doi.org/10.1103/PhysRevLett.102.073005

Tran F, Stelzl J, Blaha P (2016) Rungs 1 to 4 of DFT Jacob's ladder: Extensive test on the lattice constant, bulk modulus, and cohesive energy of solids. J Chem Phys 144:204120. https://doi.org/10.1063/1.4948636

Villaescusa LA, Bull I, Wheatley PS, Lightfoot P, Morris RE (2003) The location of fluoride and organic guests in ‘as-made’ pure silica zeolites FER and CHA. J Mater Chem 13:1978–1982. https://doi.org/10.1039/B300728F

Wells SA, Sartbaeva A (2015) GASP: software for geometric simulations of flexibility in polyhedral and molecular framework structures. Mol Simul 41:1409–1421. https://doi.org/10.1080/08927022.2015.1032277